SCIENTIFIC REPORTS

OPEN

SUBJECT AREAS:
MATERIALS SCIENCE
STRUCTURAL PROPERTIES

Received
29 October 2014

Accepted
26 January 2015

Published
2 March 2015

Correspondence and requests for materials should be addressed to M.N. (mnayak@rrcat.gov.in)

Determining Chemically and Spatially Resolved Atomic Profile of Low Contrast Interface Structure with High Resolution

Maheswar Nayak, P. C. Pradhan & G. S. Lodha

Indus Synchrotrons Utilization Division, Raja Ramanna Centre for Advanced Technology, Indore-452013 (M P), India.

We present precise measurements of atomic distributions of low electron density contrast at a buried interface using soft x-ray resonant scattering. This approach allows one to construct chemically and spatially highly resolved atomic distribution profile upto several tens of nanometer in a non-destructive and quantitative manner. We demonstrate that the method is sensitive enough to resolve compositional differences of few atomic percent in nano-scaled layered structures of elements with poor electron density differences (0.05%). The present study near the edge of potential impurities in soft x-ray range for low-Z system will stimulate the activity in that field.

Thin films and multilayers (MLs), nano-structured in one dimension, have unique optical, structural, electronic and magnetic properties with a wide range of applications[1,2]. Properties of these structures are strongly influenced by presence of small quantity of impurity, layer composition, interfacial microstructure and chemical nature[3–5]. Low electron density contrast (EDC) structures are of enormous interest. For *e.g.*, in Co/Cu magnetic MLs, presence of small magnetic impurity (*e.g.*, Ni) concentrations in the nonmagnetic (Cu) layer brings drastic changes in magnetic coupling and magnetoresistance (ref. 4). Similarly, as the size of the semiconductor structure decreases, the dopant distribution—which plays a fundamental role in determining the properties—become narrower (~nm). Establishing a microscopic picture for fundamental understanding of this narrow low-atomic number (Z) doping layer require spatial and chemical characteristics on the atomic scale[6–8]. Recently, growth of graphene on SiC and SiO_2 is of interest due to its unique physical and electronic properties and find potential applications[9]. Because of its importance, numerous efforts have been invested to characterize low contrast underlying interface structure and chemical nature which strongly influences growth and properties[10–12] using different techniques[13,14]. Again, low EDC structures with low-Z/low-Z combinations[15,16] and in particular Si/B_4C structure is of current interest due to potential application in emerging fields like astrophysics[17], low bandpass filter[18] and electronic applications[19], where the properties of these structures are strongly affected by the interfacial microstructure and atomic distribution. However, accurate understanding of atomic distribution and microstructure remain uncertain due to low contrast problem (ref. 18). Progress in understanding and predicting the properties relies on quantitative information about the distribution of these parameters at the atomic scale. So, it is clear that chemically resolved small atomic concentration and their spatial distribution across nano-scaled buried interfaces of low EDC are interesting and important aspects, and those need to be investigated.

Despite important scientific interest, quantitative precise measurement of such informations at deeply embedded interfaces are very scarce owing to the fact that there are not many techniques available to measure such a small quantity of chemically resolved atomic composition profile and microstructure wherever layer thicknesses of the order of ~ nm are involved. A combination of conventional hard x-ray reflectivity (XRR) and x-ray standing waves (XSW) analysis has been employed to quantify such a distribution[20,21] with a precision of ~2 atomic percent (at.%) and depth resolution of ~0.1 nm[22] generally from high contrast periodic ML. However, difficulty arises in XRR to probe microstructure when the EDC at an interface is low ($\Delta\rho/\rho \leq 5\%$)[23], and to extract the layer composition. For *e.g.*, in a Pt/C ML, even a 15% change in the electron density of the C-layers (say due to Pt diffusion into the C-layers) does not produce a significant change in XRR (ref. 20). So, combined XSW-XRR techniques are restricted in their success owing to lack of sensitivity in structures like: (i) For non-periodic structure and/or with low-Z materials where x-ray fluorescence signal is very weak. (ii) For low contrast interfaces because of contrast limit of XRR. Recently, a nice study has been done on mono-layers of graphene/SiC (0001) interface[24] using XSW-excited photoelectron spectroscopy, however it is a surface sensitive (~1–10 nm) tech-

nique. Indeed, here we present using resonant soft x-ray reflectivity (R-SoXR), a method that can overcome previous limitations owing it's excellent chemical sensitivity to low-Z materials, high contrast variation and high resolution. R-SoXR has been used for studying polymeric & organic materials[25–30], ionic liquid[31], electronic and structural analysis of hard matter[32–34] and magnetization in magnetic structures[35–37]. However, very little is known about it's utility to precisely measure chemically and spatially resolved atomic distribution profile across low contrast and low-Z interface structure.

In this letter, precise quantitative measurements of both chemically selective atomic concentration and their spatial distributions along the microstructure of underlying Si/B_4C interfaces are presented. We observe that there is a chemical change in B_4C and we are in position to resolve differences of few at.% of compositional variation and their spatial distribution which ultimately enables for construction of highly chemically resolved interfacial map.

Results

Hard x-ray reflectivity. Thin film samples are fabricated with varying position of B_4C layer (30Å) in Si thin film of thickness 300 Å. B_4C is at top, middle and bottom of Si layer for sample 1 (S1), sample 2 (S2) and sample 3 (S3), respectively. In all samples, a W layer of thickness 10 Å is deposited just above the Si substrate to provide an optical contrast between substrate and the film. Prior to R-SoXR measurements, hard XRR measurements are done using Cu K_α source and data are plotted upto $q_z = 0.23$ (figures 1(a) and (b)) to compare with q_z-range of R-SoXR measurements. Measured profiles of three samples with varying position of B_4C layer in Si clearly appear very similar (figure 1(a)). Inset of figure 1(a) shows also nearly identical electron density profiles (EDP) obtained from best-fit results of XRR of S1, S2 and S3 (figure 1(b)). The fitted profile matches well with the measured curve by considering Si and B_4C as a single layer having total thickness of 333 ± 1 Å; and mass density ~90 ± 2% of bulk value of Si with rms roughness ~8 ± 0.5, 7.5 ± 0.5 and 9 ± 0.5 Å; for samples S1, S2 and S3, respectively. W layer thickness is 10.5 ± 0.5 Å with mass density ~92 ± 2% of bulk value having rms roughness ~6 ± 0.5 Å for all samples. The rms roughness of the substrates is ~4.5 ± 0.5 Å. Thus, conventional XRR is not sensitive to Si/B_4C interface having low EDC, $\Delta\rho/\rho = 0.05\%$, and to compositional changes in the film, due to low contrast and lack of element-specificity.

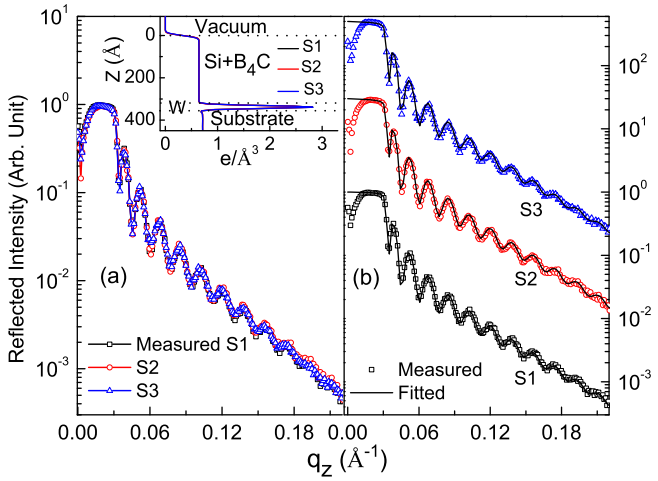

Figure 1 | (a) Overlap of measured hard XRR of three samples (S1, S2 and S3) upto $q_z = 0.23$. (b) Measured along with fitted XRR profile (vertically shifted). Inset shows EDP obtained from best-fit hard XRR results.

Sensitivity of resonant reflectivity to low contrast interface. Sensitivity of resonant reflectivity to low contrast Si/B_4C interface is demonstrated by performing repeated measurements at a selected energy of 191.4 eV (B K-edge of B_4C) (figure 2 (b)). Figure 2(a) illustrates schematic diagram of three deposited samples S1, S2 and S3 with different spatial positions of B_4C layer. To understand the observed scattered profiles for chemically selective atomic distribution analysis, the measured atomic scattering factor (ASF) of B, B_4C and B_2O_3 near boron K-edge are shown in figure 3. At this specified energy of 191.4 eV, ASF of B_4C has a strong variation (figure 3). The strong modulations in reflected spectra (figure 2 (b)) is due to major reflection contribution from Si/B_4C interface apart from contributions from other interfaces. Thus the measured profiles of three samples are significantly different, as the spatial position of B_4C layer changes in Si film. The origin of the long period oscillations in the reflectivity curve for S2 is related to the strong optical contrast at Si/B_4C where B_4C is sandwich between two Si layers resulting smaller individual Si thickness. Two vertical dotted lines mark how the period of oscillations gets modulated as position of the B_4C layer varies in Si film. This provides an experimental evidence for sensitive of R-SoXR to the spatial variation of a low contrast interface. The results demonstrated here with $\Delta\rho/\rho = 0.05\%$ as an example, has two orders of magnitude better EDC sensitivity compared to conventional hard XRR.

Spectroscopic like information using resonant reflectivity. In ion beam sputter deposited B_4C films, there may be a partial decomposition of B_4C to elementary boron (B). The elementary B on the surface is likely to react with oxygen when it is exposed to ambient conditions. The question arises whether there is a chemical change in the B_4C layers, and if so, to quantity it and to determine the elemental distribution from the surface down to a depth of ~300 Å.

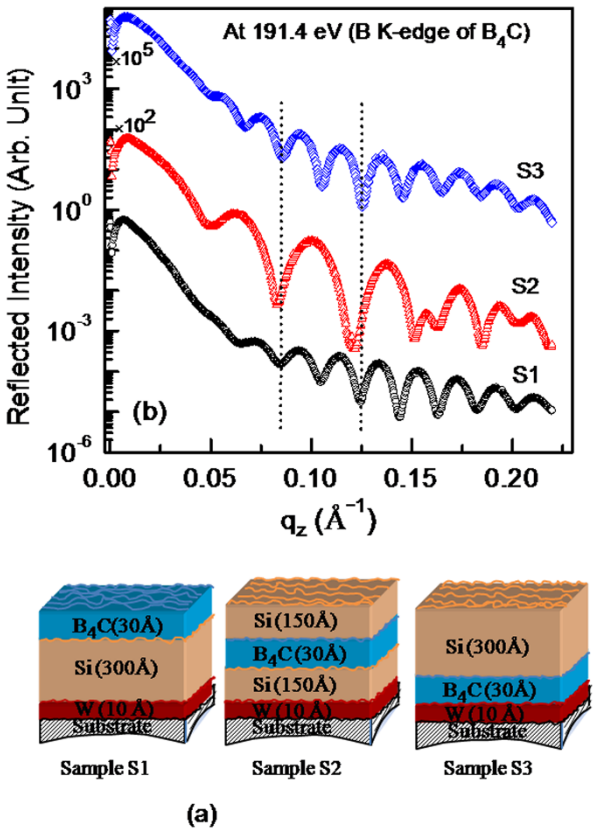

Figure 2 | (a) Schematic diagram of three fabricated samples with varying spatial positions of B_4C layer. (b) Measured R-SoXR profiles at a selected energy of 191.4 eV (B K-edge of B_4C).

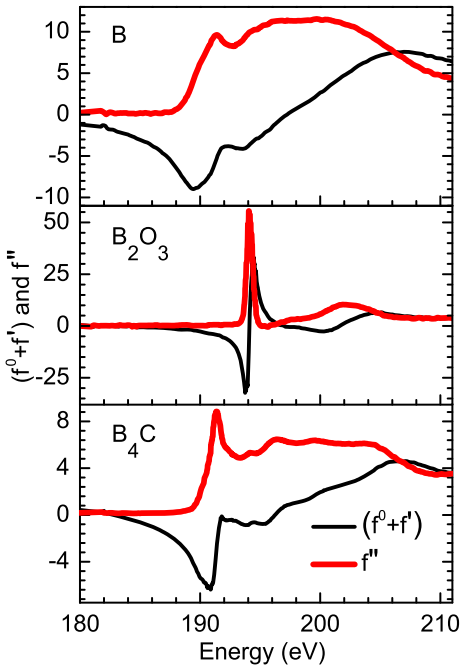

Figure 3 | Measured ASF of B, B_4C and B_2O_3 near boron K-edge to understand and correlate with the observed R-SoXR profiles.

To obtain spectroscopic like information of whether chemical changes exist in the B_4C layer or not, R-SoXR measurements are performed at selected energies near the respective absorption edge of boron and it's all the possible compounds. Figure 4(a) demonstrates experimental evidence of the presence of chemical changes in sample S1. The measurements are performed at B K-edge of both elementary B (~189.5 eV) and B_2O_3 (~194.1 eV). Near B edge, three energies of 188, 189 and 189.8 are chosen. At these energies the ASF undergoes strong variation for boron but not for B_2O_3 (figure 3). If the film contains elementary B within penetration depth of x-ray (for e.g., at 189.8 eV, penetration depth in B is ~500 Å), it will produce a strong modulation in reflected spectra as incident energy is varied in these range. However, the measured reflected spectra are clearly appear very similar near B K-edge of elementary B (figure 4(a)). This observation corroborates no elementary B is present in sample S1. The upper limit of elementary boron in sample S1 is ~3% consistent with the measurement. Similarly, to confirm the presence of B_2O_3 in sample S1, R-SoXR measurements are performed at three selected energies of 193.7, 194 and 194. 3 eV across the strong B K-absorption edge of B_2O_3. At these energies the ASF of B_2O_3 undergoes strong variation but elementary boron exhibits nearly a flat optical response (figure 3). The scattering strength of B_2O_3, $\left(f^0_{NR,B2O3}+f'_{R,B2O3}(E)\right)^2+\left(f''_{R,B2O3}(E)\right)^2$, at energies 193.7, 194 and 194. 3 eV are ~1400, 2940 and 2079, respectively which are more than three orders of magnitude higher than that of away from absorption edge (for e.g., 0.4 at 185 eV). Thus, near the edge, B_2O_3 provides enhanced and tunable scattering. In figure 4(a), near B K-edge of B_2O_3, as the energy changes from 193.7 to 194.3 eV, the measured R-SoXR curves undergo strong variation with significant change in the amplitude as well as shape of the oscillations. This corroborates presence of B_2O_3 in sample S1. These experimental results provide evidence of the chemical changes in B_4C layer which may be due to decomposition of some of B_4C during deposition. In sample S1, all the decomposed B atoms in the top B_4C layer are fully oxidized.

Chemically selective quantitative atomic profile. To quantify atomic percent of B_2O_3 and it's spatial distribution in B_4C layer of sample S1, R-SoXR measured data along with fitted profiles with

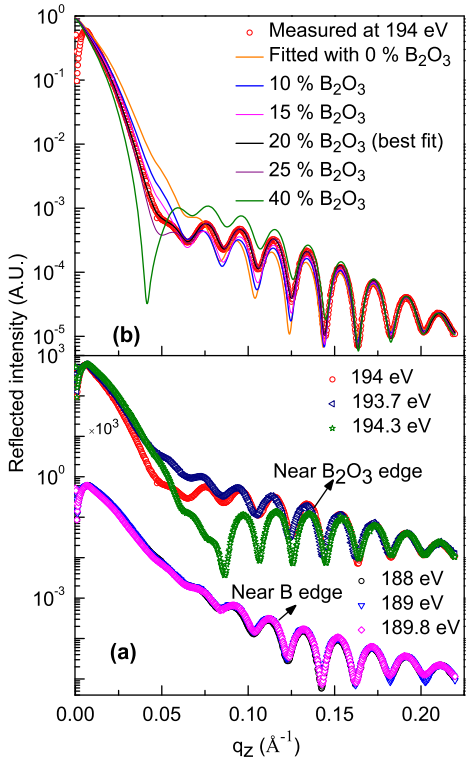

Figure 4 | (a) Measured R-SoXR profiles of sample S1 at selected energies near B K-edge of both B and B_2O_3. (b) Measured R-SoXR profile of S1 at a selected energy of 194 eV (near B_2O_3 edge) along with fitted profiles with varying atomic percent of B_2O_3 in the top B_4C layer.

different models are shown in figure 4(b). The measured data are fitted by slicing B_4C layer with different thicknesses and atomic compositions to account spatial variation of at. % of B_2O_3 within B_4C layer. However, the best-fit data matches well with the experimental data with uniform distribution model. The layer thickness and roughness obtained by simultaneous fitting measured data at different selected energies near B K-edge of B_2O_3 are kept constant. The optimized value for thickness (roughness) of Si and B_4C layers are 302 Å (9 Å) and 31 Å (8 Å), respectively. Figure 4(b) shows the variation of fitted profiles with the measured R-SoXR curve (at energy 194 eV) when the content of at. % of B_2O_3 in B_4C layer is varied. As at. % of B_2O_3 is varied from 0 to 40%, the reflected profile undergoes strong modulation producing changes in both the amplitude and shape of the oscillations envelope. Here, it is mentioned that while structural parameters are linked to the periods of the oscillations in the reflected profile, parameters of the atomic composition of the resonating atom/compound are closely related to the amplitudes and shape of the oscillations envelope. Even by mixing 5% of B_2O_3, brings significant change in optical properties of the B_4C layer (*e.g.*, δ changes from -4.53×10^{-4} to -8.33×10^{-4} and β changes from 2.62×10^{-3} to 3.41×10^{-3}) at 194 eV, which brings significant changes in reflected spectra. The scattering contrast at interface, $(\Delta\delta)^2 + (\Delta\beta)^2$, which is proportional to scattering intensity undergoes significant and tunable enhancement. In figure 4 (b), the fitted profile with 20 at. % of B_2O_3 in top B_4C layer is well matches the measured curve. The sharp and strong resonance effect provides more accuracy. The result clearly reveals resonant reflectivity is a highly sensitive technique to quantify atomic composition within a few at. % of precision.

The effective EDP (bottom panel of figure 5) is obtained from the best-fit R-SoXR curve (top panel of figure 5) at three different selected energies. The EDP undergoes gradual variation at the

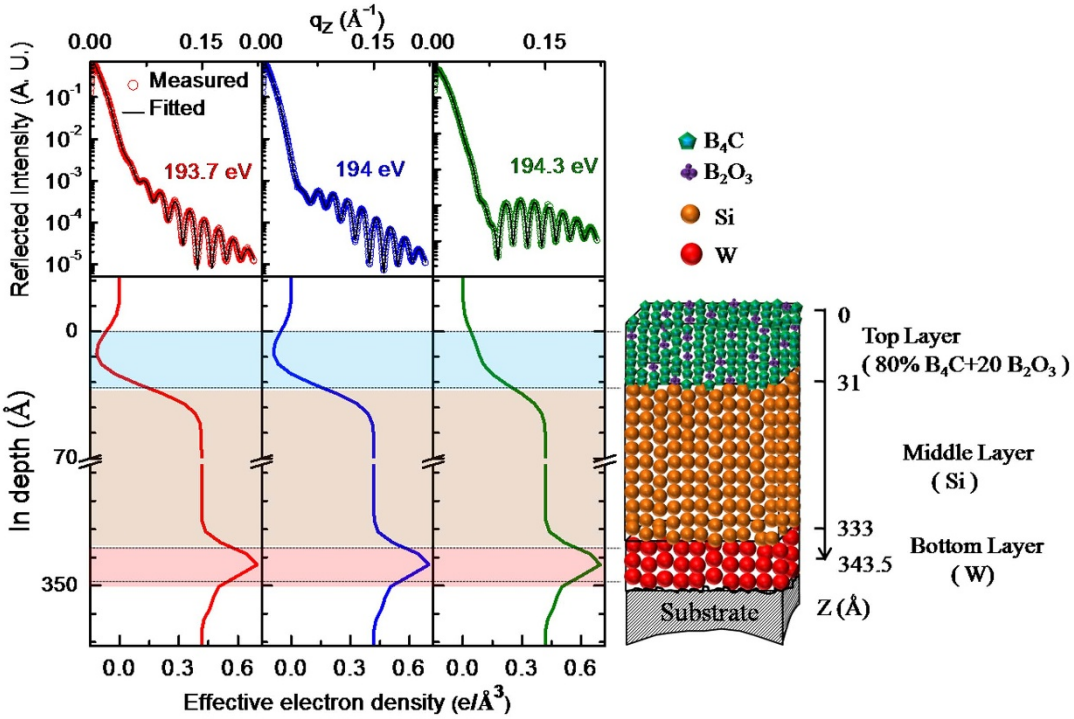

Figure 5 | Top panel shows measured R-SoXR profiles along with best-fit data of Sample S1 at selected energies near B K-edge of B_2O_3. The corresponding bottom panel shows effective EDP. The schematic diagram at right side shows an illustrative the vertical depth profile of composition profile modeled for real structure in sample S1. Size of balls is not scales to actual size of atoms and compounds.

interfaces and is sensitive to Si/B_4C interface. The EDP profiles clearly show that the position of B_4C layer is at top of Si in sample S1. The EDP of B_4C layer containing B_2O_3 undergoes significant change as the energy is tuned near B K-edge of B_2O_3. A schematic diagram representing model of vertical atomic composition distribution in different layers obtained from best-fit R-SoXR results is shown in right hand side of figure 5. The best-fit results of sample S1 are: thickness (roughness) of W, Si and B_4C layers as 10.5 ± 0.5 Å (6 ± 0.5 Å), 302 ± 1 Å (9±0.5Å) and 31 ± 0.5 Å (8 ± 0.5 Å), respectively. The best-fit results also reveal that the top B_4C layer is composed of ~80 ± 3% of B_4C and ~20 ± 3% of B_2O_3.

Similar to quantitative determination of atomic profile along with microstructure for sample S1, those of samples S2 and S3 have been also determined. The procedure for data analysis for samples S2 and S3 is similar to that of S1. In order to find spectroscopic like information of whether B_2O_3 is present in the samples S2 and S3 or not, R-SoXR measurements are performed across the very strong and sharp B K-absorption edge of B_2O_3 (figure 6). However, the measured R-SoXR profiles are nearly identical in nature at three selected energies of 193.7, 194 and 194.3 eV for both S2 and S3. R-SoXR measured data are consistent with repeating the measurements three times. This confirms B_2O_3 is not present in samples S2 and S3. The upper limit of B_2O_3 in sample S2 and S3 is ~3% consistent with measurement. The presence of elementary boron in sample S2 is confirmed by significant variation of measured R-SoXR profiles near the B K-edge of elementary boron at three selected energies of 188, 189 and 189.8 eV (figure 7). In figure 7, the fitted profile well matches the measured curve for three different energies. The best-fit results of sample S2 are: thickness (roughness) of W, bottom Si, B_4C and top Si layers as 10.5 ± 0.5 Å (6 ± 0.5 Å), 151 ± 1 Å (7.5 ± 0.5 Å), 31 ± 0.5 Å (5 ± 0.5 Å) and 151 ± 1 Å (7.5 ± 0.5 Å), respectively. The best-fit results reveal that B_4C layer is composed of ~80 ± 3% of B_4C and ~20 ± 3% of B. Similarly for sample S3, the best-fit results of R-SoXR measurements near B K-edge of elementary B are obtained as: thickness (roughness) of W, B_4C and top Si layers are 10.5 ± 0.5 Å (6 ± 0.5 Å), 31 ± 0.5 Å (5 ± 0.5 Å) and 302 ± 1 Å (9 ± 0.5 Å), respectively. The best-fit results reveal that B_4C layer is composed of ~80 ± 3% of B_4C and ~20 ± 3% of B. This clearly demonstrates the sensitivity of our measurements and novelty in the approach.

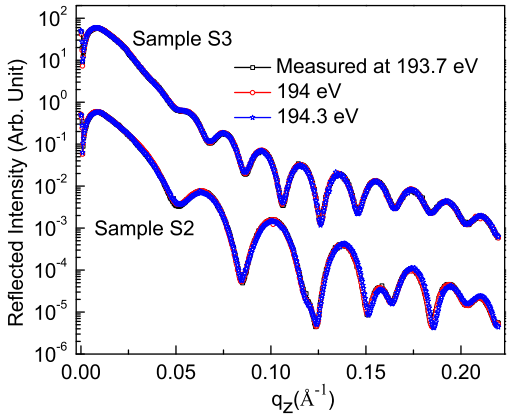

Figure 6 | Measured R-SoXR profiles at selected photon energies near B K-edge of B_2O_3 of samples S2 and S3.

Conclusion

In conclusion, we precisely measured chemically and spatially resolved atomic distribution profile with high resolution along with microstructure of the low contrast buried interfaces critical for nano-scaled layered structure devices. In prospective, methodology introduced here can be readily generalized to other complex multi-component interfaces. Structures up to several tens of nanometer thickness relevant to many scientific and technological problems can be studied. Such quantitative precise measurements help to understand properties of layered structures associated with chemically resolved interface map.

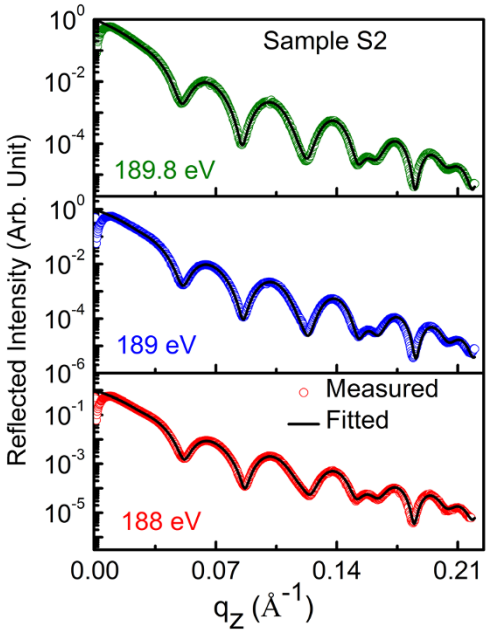

Figure 7 | Measured R-SoXR curves along with best-fit profiles of Sample S2 at selected energies near B K-edge of elementary B.

Methods

All the thin film samples are fabricated using ion beam sputtering system with base pressure of $\sim 2 \times 10^{-8}$ mbar. R-SoXR measurements are carried out in the s-polarized geometry using reflectometry beamline on Indus-1 synchrotron[38]. R-SoXR data are fitted using Parratt formalism[39]. R-SoXR data analysis requires a precise value of near edge optical constants, δ and β (refractive index $n = 1 - \delta + i\beta$), of materials and hence atomic scattering factor, $f(E) = f^0 + f'(E) - if''(E)$. Limitation of Henke optical data[40] is the lack of fine spectral details to describe optical properties near absorption edges and hence requires precise measured optical constants for R-SoXR analysis. Precise near edge optical constants for B_4C, B and B_2O_3 are obtained using the measured total electron yield absorption data[41] and using Kramers-Kronig relation. For the model fitting of R-SoXR data, the structural parameters such as substrate roughness, and W layer thickness, density and roughness obtained from hard XRR are used. Starting guess for B_4C and Si layer thickness are used as per deposited value. Measured optical constants are used for resonating materials and that of non-resonating materials are taken from Henke *et al.* (ref. 40). The mass densities used for calculation of optical constants of B, B_4C, B_2O_3, Si, and W are 2.34, 2.52, 2.46, 2.33 and 19.3 gm/cm^3, respectively.

1. Chang, L. L. & Giessen, B. C. (Eds.) *Synthetic Modulated Structure* (Academic Press, London, UK, 1985).
2. Decher, G. & Schlenoff, J. B. (Eds.) *Multilayer Thin Films* (WILEY-VCH Verlag GmbH & Co. KGaA, Weinheim, 2003).
3. Spiller, E. *Soft X-ray Optics* (SPIE Optical Engineering Press, Washington, DC, USA, 1994).
4. Parkin, S. S. P., Chappert, C. & Herman, F. Oscillatory exchange coupling and giant magnetoresistance via Cu-X alloys (X = Au, Fe, Ni). *Europhys. Lett.* **24**, 71–76 (1993).
5. Davies, A., Stroscio, A. J., Pierce, D. T. & Celotta, R. J. Atomic-scale observations of alloying at the Cr-Fe(001) interface. *Phys. Rev. Lett.* **76**, 4175–4178 (1996).
6. Johnson, M. B., Koenraad, P. M., Van der Vleuten, W. C., Salemink, H. W. M. & Wolter, J. H. Be delta-doped layers in GaAs imaged with atomic resolution using scanning tunneling microscopy. *Phys. Rev. Lett.* **75**, 1606–1609 (1995).
7. Modesti, S. *et al.* Microscopic mechanisms of self-compensation in Si δ-doped GaAs. *Phys. Rev. Lett.* **92**, 086104 (2004).
8. Hart, L., Fahy, M. R., Newman, R. C. & Fewster, P. F. X-ray characterization of Si δ-doping in GaAs. *Appl. Phys. Lett.* **62**, 2218–2220 (1993).
9. Berger, C. *et al.* Electronic confinement and coherence in patterned epitaxial graphene. *Science* **312**, 1191–1196 (2006).
10. Ohte, T. *et al.* Interlayer interaction and electronic screening in multilayer graphene investigated with angle-resolved photoemission spectroscopy. *Phys. Rev. Lett.* **98**, 206802 (2007).
11. Kim, S., Ihm, J., Choi, H. J. & Son, Y.-W. Origin of anomalous electronic structures of epitaxial graphene on silicon carbide. *Phys. Rev. Lett.* **100**, 176802 (2008).
12. Gong, Y. *et al.* Direct chemical conversion of graphene to boron- and nitrogen- and carbon- containing atomic layers. *Nature Comm.* **5**, 3193 (2014).
13. Emtsev, K. V., Speck, F., Seyller, Th., Ley, L. & Riley, J. D. Interaction, growth, and ordering of epitaxial graphene on SiC{0001} surfaces: A comparative photoelectron spectroscopy study. *Phys. Rev. B* **77**, 155303 (2008).
14. Hass, J., Millán-Otoya, J. E., First, P. N. & Conrad, E. H. Interface structure of epitaxial graphene grown on 4H-SiC(0001). *Phys. Rev. B* **78**, 205424 (2008).
15. Hau-Riege, S. P. *et al.* Subnanometer-scale measurements of the interaction of ultrafast soft x-ray Free-Electron-Laser pulses with matter. *Phys. Rev. Lett.* **98**, 145502 (2007).
16. Yan, C. *et al.* Electronic structure and electrical transport in ternary Al-Mg-B films prepared by magnetron sputtering. *Appl. Phys. Lett.* **102**, 122110 (2013).
17. Suman, M., Pelizzo, M. G., Windt, D. L. & Nicolosi, P. Extreme-ultraviolet multilayer coatings with high spectral purity for solar imaging. *Appl. Opt.* **48**, 5432–5437 (2009).
18. Slaughter, J. M. *et al.* Si/B_4C narrow-band pass mirrors for the extreme ultraviolet. *Opt Lett.* **19**, 1786–1788 (1994).
19. Adenwalla, S. *et al.* Boron carbide/*n*-silicon carbide heterojunction diodes. *Appl. Phys. Lett.* **79**, 4357–4359 (2001).
20. Ghose, S. K. & Dev, B. N. X-ray standing wave and reflectometric characterization of multilayer structures. *Phys. Rev. B* **63**, 245409 (2001).
21. Bera, S., Bhattacharjee, K., Kuri, G. & Dev, B. N. Probing atomic migration in nanostructured multilayers: Application of x-ray standing wave fields. *Phys. Rev. Lett.* **98**, 196103 (2007).
22. Ghose, S. K. *et al.* Ion-irradiation-induced mixing, interface broadening and period dilation in Pt/C multilayers. *Appl. Phys. Lett.* **79**, 467–469 (2001).
23. Seeck, O. H. *et al.* Analysis of x-ray reflectivity data from low-contrast polymer bilayer systems using a Fourier method. *Appl. Phys. Lett.* **76**, 2713–2715 (2000).
24. Emery, J. D. *et al.* Chemically resolved interface structure of epitaxial graphene on SiC(0001). *Phys. Rev. Lett.* **111**, 215501 (2013).
25. Wang, C., Araki, T. & Ade, H. Soft x-ray resonant reflectivity of low-*z* material thin films. *Appl. Phys. Lett.* **87**, 214109 (2005).
26. Araki, T. *et al.* Resonant soft x-ray scattering from structured polymer nanoparticles. *Appl. Phys. Lett.* **89**, 124106 (2006).
27. Mitchell, G. E. *et al.* Molecular bond selective x-ray scattering for nanoscale analysis of soft matter. *Appl. Phys. Lett.* **89**, 044101 (2006).
28. Collins, B. A. *et al.* Polarized x-ray scattering reveals non-crystalline orientational ordering in organic films. *Nature Materials* **11**, 536–543 (2012).
29. Pasquali, L. *et al.* Structural and electronic properties of anisotropic ultrathin organic films from dichroic resonant soft x-ray reflectivity. *Phys. Rev. B* **89**, 045401 (2014).
30. Yan, H., Wang, C., McCarn, A. R. & Ade, H. Accurate and facile determination of the index of refraction of organic thin films near the carbon 1s absorption edge. *Phys. Rev. Lett.* **110**, 177401 (2013).
31. Mezger, M., Ocko, B. M., Reichert, H. & Deutsch, M. Surface layering and melting in an ionic liquid studied by resonant soft x-ray reflectivity. *PNAS* **110**, 3733–3737 (2013).
32. Park, J. *et al.* Oxygen-vacancy-induced orbital reconstruction of Ti ions at the interface of LaAlO3/SrTiO3 heterostructures: A resonant soft-x-ray scattering study. *Phys. Rev. Lett.* **110**, 017401 (2013).
33. Valvidares, S. M., Huijben, M., Yu, P., Ramesh, R. & Kortright, J. B. Native SrTiO3 (001) surface layer from resonant Ti L2,3 reflectance spectroscopy. *Phys. Rev. B* **82**, 235410 (2010).
34. Nayak, M., Lodha, G. S., Sinha, A. K., Nandedkar, R. V. & Shivashankar, S. A. Determination of interlayer composition at buried interfaces using soft x-ray resonant reflectivity. *Appl. Phys. Lett.* **89**, 181920 (2006).
35. Tonnerre, J.-M. *et al.* Soft x-ray resonant magnetic scattering from a magnetically coupled Ag/Ni multilayer. *Phys. Rev. Lett.* **75**, 740–743 (1995).
36. Tonnerre, J.-M. *et al.* Depth magnetization profile of a perpendicular exchange coupled system by soft-x-ray resonant magnetic reflectivity. *Phys. Rev. Lett.* **100**, 157202 (2008).
37. Benckiser, E. *et al.* Orbital reflectometry of oxide heterostructures. *Nature Materials* **10**, 189–193 (2011).
38. Lodha, G. S., Modi, M. H., Raghuvanshi, Sawhney, K. J. S. & Nandedkar, R. V. Soft x-ray reflectometer on Indus-1. *Synchrotron Radiation News* **17**, 33–35 (2004).
39. Parratt, L. G. Surface studies of solids by total reflection of x-rays. *Phys. Rev.* **95**, 359–369 (1954).
40. Henke, B. L., Gullikson, E. M. & Davis, J. C. X-ray interactions: Photoabsorption, scattering, transmission, and reflection at E = 50–30,000 eV, Z = 1–92. *At. Data and Nucl. Data Tables* **54**, 181–342 (1993).
41. Li, D., Bancroft, G. M. & Fleet, M. E. B K-edge XANES of crystalline and amorphous inorganic materials. *J. Electron Spectrosc. Relat. Phenom.* **79**, 71–73 (1996).

Acknowledgments

The authors sincerely acknowledge Dr. M. H. Modi for soft x-ray reflectivity measurements. The authors thank Dr. Dien Li to provide us absorption data. Authors also sincerely acknowledge Prof. H. Ade, Prof. J. Zegenhagen, Prof. U. Pietsch, Prof. J. M. Tonnerre, Prof. B. M. Ocko and Prof. T. Koga for helpful discussions.

Author contributions

M.N. took part in conceiving the idea and performed experiments; M.N., G.S.L. and P.C.P. discussed the results; M.N. wrote the manuscript; All authors reviewed the manuscript.

Additional information

Competing financial interests: The authors declare no competing financial interests.

How to cite this article: Nayak, M., Pradhan, P.C. & Lodha, G.S. Determining Chemically and Spatially Resolved Atomic Profile of Low Contrast Interface Structure with High Resolution. *Sci. Rep.* **5**, 8618; DOI:10.1038/srep08618 (2015).

SCIENTIFIC REPORTS

OPEN

Corrigendum: Determining Chemically and Spatially Resolved Atomic Profile of Low Contrast Interface Structure with High Resolution

Maheswar Nayak, P. C. Pradhan, G. S. Lodha, A. Sokolov & F. Schäfers

Scientific Reports **5**:8618; doi: 10.1038/srep08618; published online 02 March 2015; updated 11 July 2016

It was brought to the authors' attention that the original paper contains the following errors. (i) We reported a 0.05% electron density contrast between silicon and boron carbide. There was a calculation error in computing this number and the correct contrast is 0.5%. This is one order of magnitude lower than what can be studied using hard x-ray reflectivity. Therefore, with this revised electron density contrast value, the proposed methodology is still valid. (ii) Numerical errors were made during the conversion of the measured angular reflectivity to q_z ($4\pi \sin\theta/\lambda$). To revalidate the proposed methodology, we have performed fresh measurements on similar new samples. The fresh soft x-ray resonant reflectivity measurements were done using the Optics Beamline at the BESSY storage ring which has a better energy resolution ($E/\Delta E \cong 670$), smaller vertical angular divergence (0.5 mrad), larger photon flux ($\sim 1.4 \times 10^{10}$) and accessible q-space compared to the measurements reported in the original paper using the Indus -1 reflectivity beamline. The results are presented below and the methodology and the conclusion reported in the original paper still stand.

Hard x-ray reflectivity. Thin film samples are fabricated with varying position of B_4C layer (40 Å) in Si thin film of thickness 300 Å. The samples are fabricated using electron beam evaporation. Elementary boron is incorporated into B_4C layer by co-deposition. B_4C is at top, middle and bottom of Si layer for sample 1 (S1), sample 2 (S2) and sample 3 (S3), respectively. In all samples, a W layer of thickness 10 Å is deposited just above the Si substrate to provide an optical contrast between substrate and the film. Prior to R-SoXR measurements, hard XRR measurements are done using Cu K_α source. Hard XRR profile of all three samples are measured and fitted up to $q_z = 0.42$ Å^{-1} (theta = 3 degree). However, hard XRR profile are plotted up to $q_z = 0.22$ Å^{-1} (theta = 1.545 degree) [Figure 1(a,b)]. Measured profiles of three samples with varying position of B_4C layer in Si clearly appear very similar [Figure 1(a)]. Inset of Figure 1(a) shows nearly identical electron density profiles (EDP) obtained from best-fit results of XRR of S1, S2 and S3 [Figure 1(b)]. The fitted profile matches the measured curve by considering Si and B_4C as a single layer. The total thickness of (Si + B_4C) is 350 ± 1, 352 ± 1 and 353 ± 1 Å; and mass density is about $95 \pm 2\%$ of bulk value of Si with rms roughness = 7.5 ± 0.5, 6.5 ± 0.5 and 7 ± 0.5 Å; for samples S1, S2 and S3, respectively. W layer thickness is ~10 Å having rms roughness = 3.5 ± 0.5, 4 ± 0.5 and 4.5 ± 0.5 Å; for samples S1, S2 and S3, respectively. The rms roughness of the substrates is 4.5 ± 0.5 Å. A silicon oxide layer of thickness ~15.5 Å is considered above the silicon substrate. Thus, conventional XRR is not sensitive to Si/B_4C interface having low electron density contrast (EDC), $\Delta\rho/\rho = 0.5\%$, and to compositional variation in the film, due to low contrast and lack of element-specificity.

Sensitivity of resonant reflectivity to low contrast interface. Sensitivity of resonant reflectivity to low contrast Si/B_4C interface is demonstrated by performing measurements at a selected energy of 191.4 eV (B K-edge of B_4C) [Figure 2(b)]. Soft x-ray reflectivity measurements are carried out in the s-polarization geometry using the Optics Beamline at the BESSY-II storage ring[1,2]. The measurements were done with a better energy resolution, photon flux, accessible q-space and lower angular divergence than the measurements presented in the original paper. For the soft x-ray measurements, the data are collected up to theta = 89.2 degree. The reflectometer used was specially designed for measurements in near-normal incidence geometry. A GaAsP-photodiode

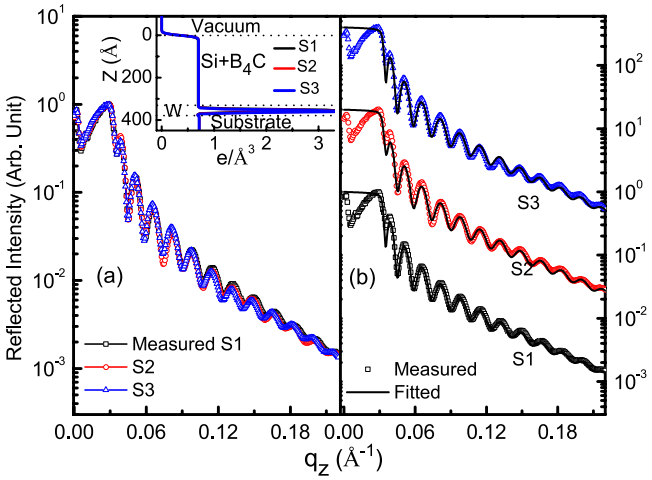

Figure 1. (**a**) Overlap of measured hard XRR of three samples (S1, S2 and S3) up to $q_z = 0.22$. (**b**) Measured along with fitted XRR profile (vertically shifted). Inset shows EDP obtained from best-fit hard XRR results.

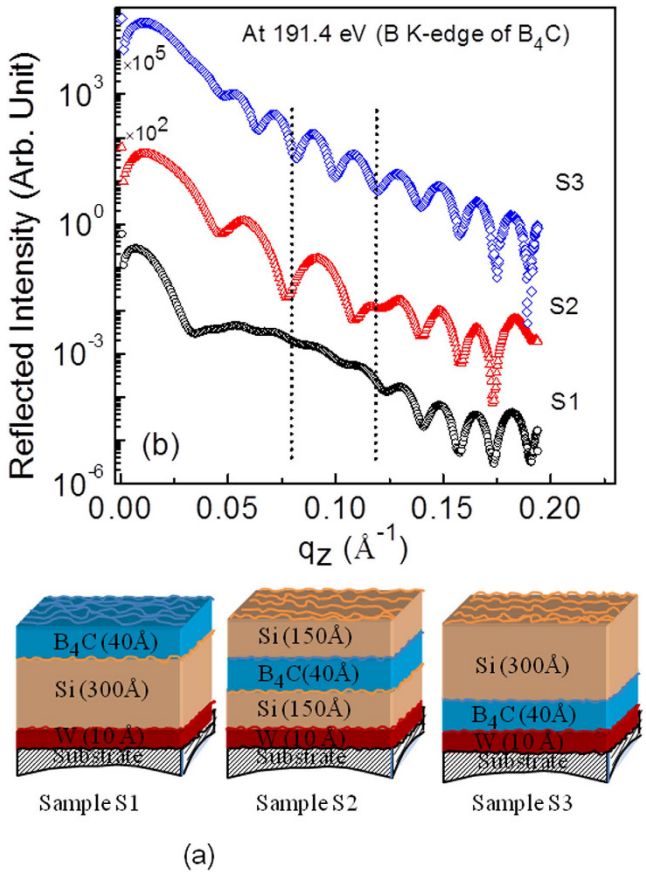

Figure 2. (**a**) Schematic of three fabricated samples with varying spatial positions of B_4C layer. Surface roughness is represented by the undulating lines. (**b**) Measured R-SoXR profiles at a selected energy of 191.4 eV (B K-edge of B_4C).

of 4 × 4 mm2 acceptance area, surrounded by a support of 2 mm diameter at a distance of 310 mm from the sample was used. The minimum angle to normal is thus atan(4/310) = 0.74°, corresponding to 89.26° grazing angle. Figure 2(a) illustrates schematic of three deposited samples S1, S2 and S3 with different spatial positions of B_4C layer. To understand the observed scattered profiles for chemically selective atomic distribution analysis, the measured atomic scattering factor (ASF) of B, B_4C and B_2O_3 near boron K-edge are shown in Figure 3. At this specified energy of 191.4 eV, ASF of B_4C has a strong variation [Figure 3]. The strong modulations in reflected spectra [Figure 2(b)] is due to major reflection contribution from Si/B_4C interface apart from contributions from

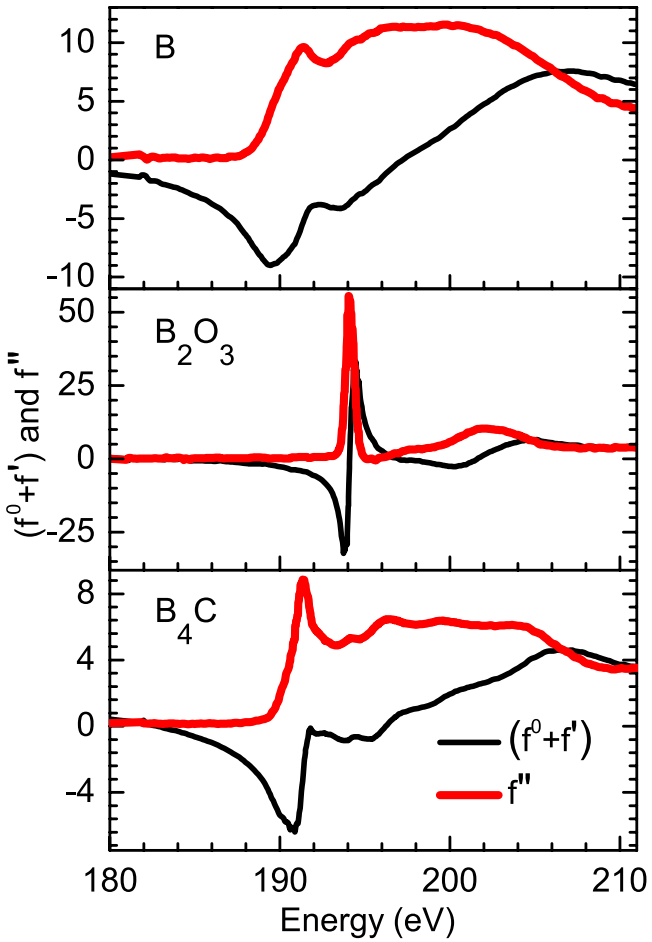

Figure 3. Measured ASF of B, B_4C and B_2O_3 near boron K-edge to understand and correlate with the observed R-SoXR profiles.

other interfaces. Due to the contribution of the reflection from the Si/B_4C interface, the three different layer structures of three samples (S1, S2 and S3) exhibit significantly different measured profiles with a strong modulation, as the spatial position of B_4C layer changes in Si film. Two vertical dotted lines mark how the period of oscillations gets modulated as position of the B_4C layer varies in Si film. This provides an experimental evidence for sensitivity of resonant soft x-ray reflectivity (R-SoXR) to the spatial variation of a low contrast interface. The results demonstrated here with $\Delta\rho/\rho = 0.5\%$ as an example, has one order of magnitude better EDC sensitivity compared to conventional hard XRR[3].

Spectroscopic information using resonant reflectivity. To determine the spectroscopic information using R-SoXR, elementary boron is introduced in B_4C layer by co-deposition using electron beam evaporation method. R-SoXR measurements are performed at selected energies near the respective absorption edges of boron and the compounds of boron. Figure 4(a) demonstrates experimental evidence of the presence of chemical changes in sample S1. The measurements are performed at B K-edge of both elementary B (~189.5 eV) and B_2O_3 (~194.1 eV). Near B K-edge of B_2O_3, four energies of 193.7, 194, 194. 3 and 194.6 eV are chosen across the edge. At these energies the ASF undergoes strong variation for B_2O_3 but elementary boron exhibits nearly a flat optical response [Figure 3]. If the film contains B_2O_3 within penetration depth of x-ray, it will produce a strong modulation in reflected spectra as incident energy is varied in these ranges. The measured reflection spectra clearly appear very similar near B K-edge of B_2O_3 [Figure 4(a)]. This observation corroborates that no B_2O_3 is present in sample S1. Similarly, to confirm the presence of B in sample S1, R-SoXR measurements are performed across the B K-absorption edge of B at selected energies of 185, 186,187, 188, 189, 190.7 and 191.4 eV [Figure 4(a)]. At these energies the ASF undergoes strong variation for boron but not for B_2O_3 [Figure 3]. Near the edge, B provides enhanced and tunable scattering. B_4C also exhibits variation of ASF with energy towards higher side with respect to elementary B. However, the magnitude of variation of ASF is more in B than B_4C due to stronger resonance enhancement of elementary B than B in B_4C. The observed changes in the reflected profile at the selected energies across the B K-edge of elementary boron can be due to contribution of both kinds of atoms. At the lower energy side, the variation in the measured profiles is dominated by the contribution of elementary boron. The contribution of B_4C starts at higher energy along with elementary boron. This corroborates the presence of B in sample S1. In the original paper, the elementary boron was not detected in S1, as elementary boron is fully oxidized when

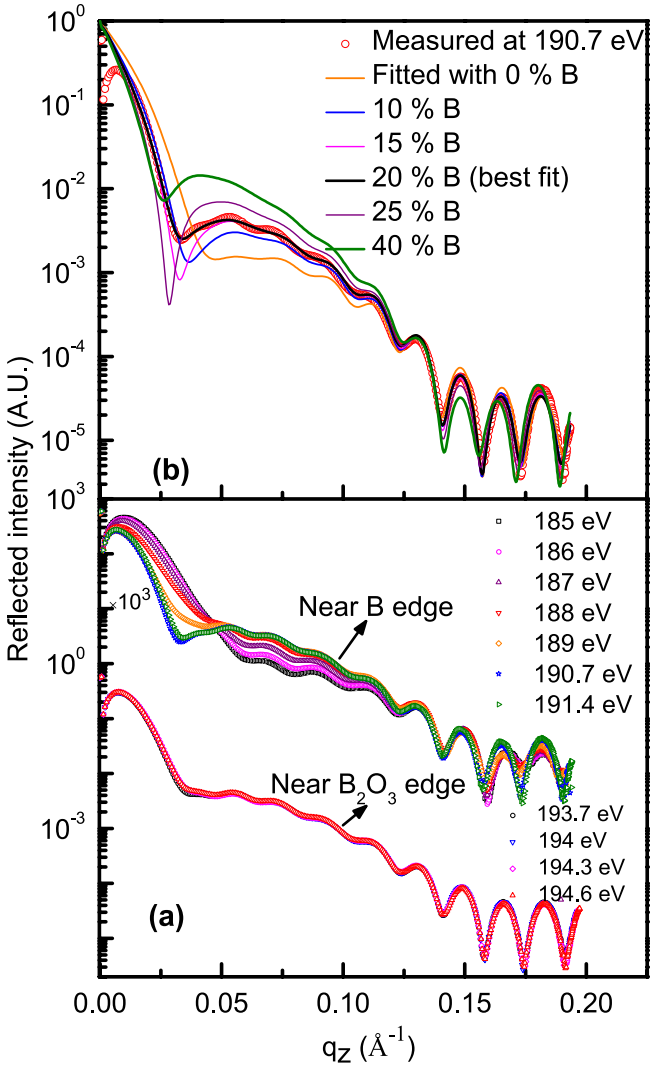

Figure 4. (**a**) Measured R-SoXR profiles of sample S1 at selected energies near B K-edge of both B and B_2O_3. (**b**) Measured R-SoXR profile of S1 at a selected energy of 190.7 eV (near B edge) along with fitted profiles with varying atomic percentage of B in the B_4C layer.

exposed to ambient condition. Whereas in the fresh sample S1 (in corrigendum), the elementary boron in the top B_4C layer is not oxidized because of a contaminated carbon layer at the top. This contaminated carbon layer most likely prevents elementary boron in the top B_4C layer to be oxidized in fresh sample S1.

Chemically selective quantitative atomic profile. To quantify the atomic percentage of B and the spatial distribution in B_4C layer of sample S1, R-SoXR measured data along with fitted profiles with different models are shown in Figure 4(b). The measured data are fitted by slicing B_4C layer with different thicknesses and atomic compositions to account for a spatial variation of at. % of B within B_4C layer. However, the best-fit data matches well with the experimental data with uniform distribution model. The layer thickness and roughness obtained by simultaneous fitting measured data at different selected energies near B K-edge of B are kept constant. The optimized value for thickness (roughness) of Si and B_4C layers are 294 Å (5 Å) and 42 Å (13 Å), respectively. An intermixing layer at the Si/B_4C interface is considered with thickness 11.5 Å and roughness 7.5 Å. A carbon contaminated layer with thickness 11.5 Å and roughness 6.5 Å is also considered at the top of B_4C layer. Figure 4(b) shows the variation of fitted profiles with the measured R-SoXR curve (at energy 190.7 eV) when the content of atomic % of B in B_4C layer is varied. As B is varied from 0 to 40%, the reflected profile undergoes strong modulation producing changes in both the amplitude and shape of the oscillations envelope. Here, it is mentioned that while structural parameters are linked to the periods of the oscillations in the reflected profile, parameters of the atomic composition of the resonating atom/compound are closely related to the amplitudes and shape of the oscillations envelope. Resonant x-ray reflectivity has excellent chemical sensitivity to the resonating atom along with their spatial distribution. This high sensitivity determines the chemically and spatially resolved atomic profile within the nanometer range with a very tiny volume of contributing material. The significant change in reflectivity profile at around $q = 0.05$ Å^{-1} by varying percent of elementary B in Figure 4(b) could be due to type of layer structure chosen in the thin film for the case study, the optical properties of the resonating atom and change in

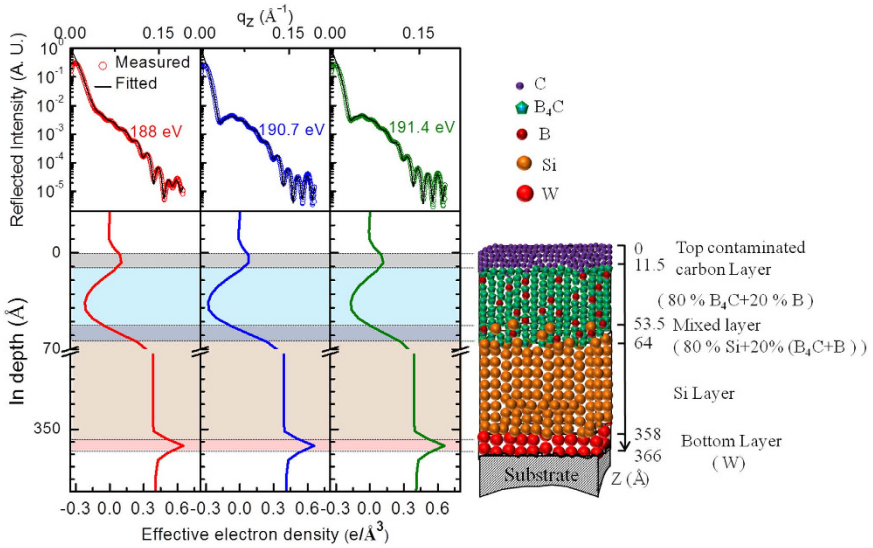

Figure 5. Top panel shows measured R-SoXR profiles along with best-fit data of Sample S1 at selected energies near B K-edge of elementary boron. The corresponding bottom panel shows effective EDP. The schematic at the right side shows the vertical depth profile of the composition modeled for the real structure in sample S1. Size of balls does not scale to the actual size of atoms and compounds.

optical contrast by varying with atomic percent of B. The changes in the values of atomic scattering factor/optical constant (δ and β) by incorporation of different percent of B in B_4C layer are as follows: At 190.7 eV, the values of δ and β of B_4C layer with 0%, 10%, 15%, 20%, 25% and 40% of B are as follows: -3.17×10^{-3} and 2.29×10^{-3}, -4.72×10^{-3} and 4.09×10^{-3}, -5.49×10^{-3} and 4.99×10^{-3}, -6.27×10^{-3} and 5.89×10^{-3}, -7.04×10^{-3} and 6.78×10^{-3}, and -9.36×10^{-3} and 9.48×10^{-3}, respectively. Even by mixing 5% of B, brings significant changes in the optical properties of the B_4C layer, which brings significant changes in the reflected spectra as well. The scattering contrast at interface, $(\Delta\delta)^2 + (\Delta\beta)^2$, which is proportional to scattering intensity undergoes significant and tunable enhancement. In Figure 4(b), the fitted profile with 20 atomic % of B in the B_4C layer matches the measured curve well. The result clearly reveals resonant reflectivity is a highly sensitive technique to quantify atomic composition within a few atomic % of the precision.

The effective EDP [bottom panel of Figure 5] is obtained from the best-fit R-SoXR curve [top panel of Figure 5] at three different selected energies. The EDP undergoes gradual variation at the interfaces and is sensitive to the Si/B_4C interface. The EDP profiles clearly show that the position of B_4C layer is at top of Si in sample S1. The EDP of B_4C layer containing B undergoes significant changes as the energy is tuned near the B K-edge of elementary boron due to the contribution of both types of B atoms (i.e. elementary B and B in B_4C) at these energies. A schematic model of the vertical atomic composition distribution in different layers obtained from best-fit R-SoXR results is shown in the right hand side of Figure 5. The best-fit results of sample S1 are: average thickness (roughness) of W, Si, interlayer (mixed layer) (B_4C-on-Si), B_4C and the top contaminated carbon layers as 8 ± 1 Å (3.5 ± 0.5 Å), 294 ± 1 Å (5 ± 0.5 Å), 11.5 ± 1 Å (7.5 ± 0.5 Å), 42 ± 1 Å (13 ± 0.5 Å) and 11.5 ± 1 Å (6.5 ± 0.5 Å), respectively. The best-fit results also reveal that the B_4C layer is composed of $80 \pm 3\%$ of B_4C and $20 \pm 3\%$ of B. The interlayer (mixed layer) is composed of 80% of Si and 20% of (80% B_4C + 20% B).

Similar to quantitative determination of the atomic profile along with microstructure for sample S1, those of samples S2 and S3 have been also determined. The procedure for data analysis for samples S2 and S3 is similar to that of S1. In order to find spectroscopic information of whether B_2O_3 is present in the samples S2 and S3 or not, R-SoXR measurements are performed across the very strong and sharp B K-absorption edge of B_2O_3 [Figure 6]. However, the measured R-SoXR profiles are nearly identical in nature at four selected energies of 193.7, 194, 194.3 and 194.6 eV for both S2 and S3. This confirms that B_2O_3 is not present in samples S2 and S3. The presence of elementary boron in sample S2 is confirmed using the procedure followed for sample S1 (discussed earlier) by performing R-SoXR measurements across the B K-edge of elementary boron at the selected energies of 185, 186, 187, 188, 190.7 and 191.4 eV. To quantify the atomic % of B and the spatial distribution in B_4C layer of sample S2, R-SoXR measured data along with best-fit profiles at three selected energies of 188, 190.7 and 191.4 eV are shown in Figure 7. The best-fit results of sample S2 are: average thickness (roughness) of W, Si, interlayer layer I (B_4C-on-Si), B_4C, interlayer II (Si-on-B_4C) and Si layers as 8 ± 1 Å (4 ± 0.5 Å), 138 ± 1 Å (8.5 ± 0.5 Å), 13 ± 1 Å (4 ± 0.5 Å), 41 ± 1 Å (6.5 ± 0.5 Å), 13 ± 1 Å (5.5 ± 0.5 Å) and 148 ± 1 Å (7 ± 0.5 Å), respectively. The best-fit results also reveal that the B_4C layer is composed of $80 \pm 3\%$ of B_4C and $20 \pm 3\%$ of B. The interlayer (mixed layer) is composed of 80% of Si and 20% of (80% B_4C + 20% B).

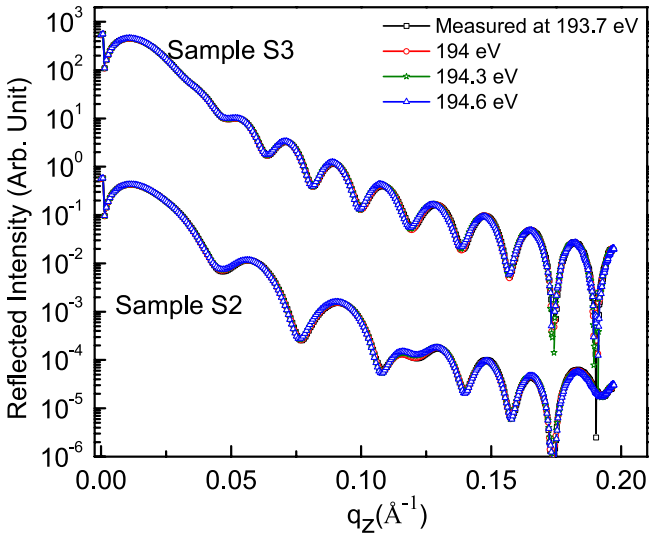

Figure 6. Measured R-SoXR profiles at selected photon energies near the B K-edge of B_2O_3 of samples S2 and S3.

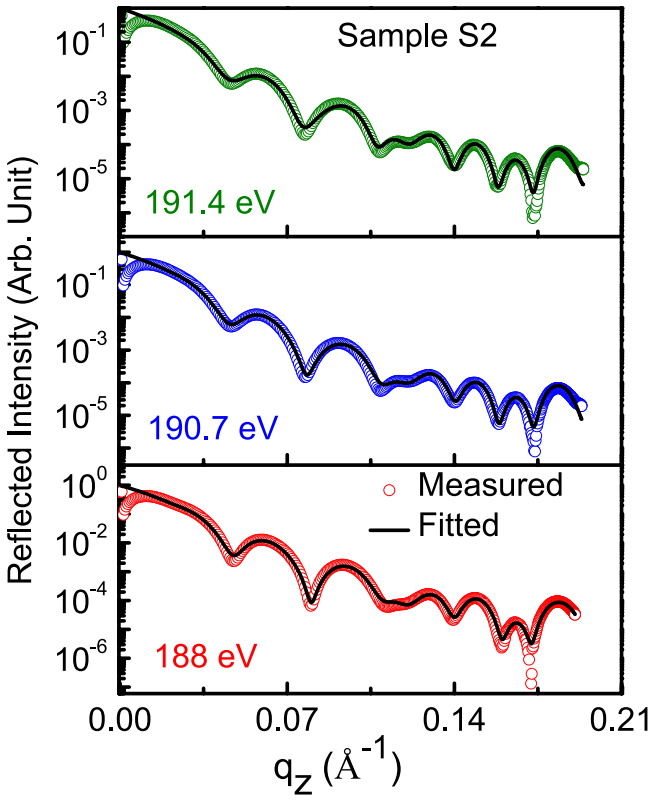

Figure 7. Measured R-SoXR curves along with best-fit profiles of sample S2 at selected energies near the B K-edge of elementary B.

Similarly for sample S3, the best-fit results of R-SoXR measurements near the B K-edge of elementary B are obtained as: average thickness (roughness) of W, B_4C, interlayer (Si-on-B_4C) and Si layers as 8 ± 1 Å (5 ± 0.5 Å), 41 ± 1 Å (5.5 ± 0.5 Å), 12 ± 1 Å (6 ± 0.5 Å) and 301 ± 1 Å (7.5 ± 0.5 Å), respectively. The best-fit results also reveal that the B_4C layer is composed of $80 \pm$ 3% of B_4C and 20 ± 3% of B. The interlayer (mixed layer) is composed of 80% of Si and 20% of (80% $B_4C + 20$% B).

Energy resolution of the measurements. The energy resolution ($E/\Delta E$) for the energy scan to determine $(f^0 + f')$ and f'' values is about 1000 at 200 eV. The energy resolution available for the angular scan, in the original paper is about 250 at 190 eV and in the corrigendum is ~670 at 190 eV with spectral impurity ~0.1%. In

the original paper, due to intensity reasons the energy resolution used for the angular scan was poorer than for the energy scan. This may lead to some uncertainty for the determination of the composition. In the original paper, to better understand the changes in reflectivity profile in the vicinity of the B K-edge of B_2O_3 (Figure 4(a) in the original paper) although the energy resolution was not optimum, we compare the changes in the value of $(f^0 + f')$ and f'' in energy interval of 0.3 eV at selected energies, below the edge (away from the edge) and near the edge. For example, as per the energy scan, below the edge, $(f^0 + f')$ and f'' of B_2O_3 are -1.71 and 0.488 at 188.5 eV, and -1.74 and 0.476 at 188.8 eV, respectively. Below the edge, the change in $(f^0 + f')$ and f'' in energy interval of 0.3 eV is small. However, near the edge, $(f^0 + f')$ and f'' of B_2O_3 are -30.46 and 13.89 at 193.7 eV, -16.3 and 49.25 at 194 eV, and 25.5 and 39.78 at 194.3 eV, respectively. Taking into account the broadening of the resonance for the angular scan in the original paper, near the edge, $(f^0 + f')$ and f'' of B_2O_3 are -27.77 and 17.53 at 193.7 eV, -15.93 and 40.44 at 194 eV, and 18.25 and 38.91 at 194.3 eV, respectively. Near the edge, the change in $(f^0 + f')$ and f'' in energy interval of 0.3 eV is significant. The variation of the atomic scattering factor of B_2O_3 near the B_2O_3 edge provides changes in the reflectivity profile as observed in the original paper.

A. Sokolov and F. Schäfers have been added to the author list because they contributed to the experiments reported in this Corrigendum. This has now been corrected in the HTML versions of the Article. The Author Contributions section in the HTML version now reads:

M.N. took part in conceiving the idea and performed experiments in the original paper; M.N., G.S.L. and P.C.P. discussed the results; M.N. wrote the manuscript; All authors reviewed the manuscript; In the corrigendum, A. S. And F. S. played a key role in the soft x-ray measurements and optimization of the beamlines for these measurements; All the authors discussed the results in preparing the scientific contents of the manuscript; M.N. wrote the manuscript; All authors reviewed the manuscript.

References

1. Sokolov, A. A., Eggenstein, F., Erko, A., Follath, R., Künstner, S., Mast, M., Schmidt, J. S., Senf, F., Siewert, F., Zeschke, T. & Schäfers, F. An XUV Optics Beamline at BESSY II. *Proc. of SPIE* **9206,** "Advances in Metrology for X-Ray and EUV Optics V", 92060J-1-13 (2014). (doi: 10.1117/12.2061778).
2. Schäfers, F., Bischoff, P., Eggenstein, F., Erko, A., Gaupp, A., Künstner, S., Mast, M., Schmidt, J. –S., Senf, F., Siewert, F., Sokolov, A. & Zeschke, Th. The At-wavelength metrology facility for UV- and XUV-reflection and diffraction optics at BESSY-II. *Journal of Synchrotron Radiation*, Proc. Of PhotonDiag Workshop Trieste **23(1),** 67–77 (2016). (http://dx.doi.org/10.1107/S1600577515020615).
3. Seeck, O. H. *et al.* Analysis of x-ray reflectivity data from low-contrast polymer bilayer systems using a Fourier method. *Appl. Phys. Lett*. **76,** 2713–2715 (2000).

SCIENTIFIC REPORTS

OPEN

Erratum: Determining Chemically and Spatially Resolved Atomic Profile of Low Contrast Interface Structure with High Resolution

Maheswar Nayak, P. C. Pradhan, G. S. Lodha, A. Sokolov & F. Schäfers

Scientific Reports **5**:8618; doi: 10.1038/srep08618; published online 02 March 2015; updated 25 August 2016

In this Article, A. Sokolov & F. Schäfers are incorrectly listed as being affiliated with 'Indus Synchrotrons Utilization Division, Raja Ramanna Centre for Advanced Technology, Indore-452013 (M P), India'. The correct affiliation is listed below:

Helmholtz-Zentrum Berlin (HZB) BESSY II, Institute f. Nanometre Optics and Technology, Albert-Einstein-Strasse 15, D-12489 Berlin, Germany.